Molecular assemblies of the catalytic domain of SOS with KRas and oncogenic mutants

Zahra Moghadamchargari[a], Mehdi Shirzadeh[a], Chang Liu[b], Samantha Schrecke[a], Charles Packianathan[a], David H. Russell[a], Minglei Zhao[b], and Arthur Laganowsky[a,1]

[a]Department of Chemistry, Texas A&M University, College Station, TX 77843; and [b]Department of Biochemistry and Molecular Biology, University of Chicago, Chicago, IL 60637

Edited by Frank McCormick, University of California, San Francisco, CA, and approved February 17, 2021 (received for review October 26, 2020)

Ras is regulated by a specific guanine nucleotide exchange factor Son of Sevenless (SOS), which facilitates the exchange of inactive, GDP-bound Ras with GTP. The catalytic activity of SOS is also allosterically modulated by an active Ras (Ras–GTP). However, it remains poorly understood how oncogenic Ras mutants interact with SOS and modulate its activity. Here, native ion mobility–mass spectrometry is employed to monitor the assembly of the catalytic domain of SOS (SOS^{cat}) with KRas and three cancer-associated mutants (G12C, G13D, and Q61H), leading to the discovery of different molecular assemblies and distinct conformers of SOS^{cat} engaging KRas. We also find $KRas^{G13D}$ exhibits high affinity for SOS^{cat} and is a potent allosteric modulator of its activity. A structure of the $KRas^{G13D}$•SOS^{cat} complex was determined using cryogenic electron microscopy providing insight into the enhanced affinity of the mutant protein. In addition, we find that $KRas^{G13D}$–GTP can allosterically increase the nucleotide exchange rate of KRas at the active site more than twofold compared to KRas–GTP. Furthermore, small-molecule Ras•SOS disruptors fail to dissociate $KRas^{G13D}$•SOS^{cat} complexes, underscoring the need for more potent disruptors. Taken together, a better understanding of the interaction between oncogenic Ras mutants and SOS will provide avenues for improved therapeutic interventions.

cancer | Ras proteins | native mass spectrometry | Ras-SOS

Ras, a member of the small G-protein family, represents important signaling molecules with diverse cellular roles, such as cell differentiation and proliferation (1–4). Different isoforms of Ras (HRas, KRas, and NRas) have high overall sequence identity and are the most commonly mutated of all discovered oncogenes (5, 6). Of the three Ras isoforms, KRas is the most frequently mutated isoform in cancers, such as pancreatic cancer (70–90%), colon cancer (30–50%), and lung cancer (20–30%) (7, 8). Ras proteins regulate cell signaling pathways by cycling between inactive, GDP-bound, and active, GTP-bound states that is accompanied by remodeling of three key regions within Ras: p-loop (residues 10–17), switch I (residues 30–38), and switch II (residues 60–76) (9–11).

As Ras proteins possess slow guanine nucleotide exchange rates, their activation is regulated by guanine nucleotide exchange factors (GEFs) that reload Ras with GTP (12, 13). The multidomain protein, Son of Sevenless (SOS), is a GEF with the cdc25 and Ras exchanger motif domains representing the minimal, functionally competent unit, termed SOS^{cat} (14). Structural studies have revealed two Ras binding sites to SOS^{cat}, leading to the discovery that binding of Ras–GTP at the distal (or allosteric) site allosterically modulates SOS^{cat} activity, which markedly increases the nucleotide exchange rate at the active site (14, 15). In addition, the degree of this allosteric modulation greatly depends on the nucleotide-bound state of Ras (14, 16, 17). Moreover, SOS is conformationally dynamic and binding of Ras at the allosteric site appears to shift the population to active conformation(s) of SOS (18). In addition, SOS^{cat} samples a broad range of turnover rates by fluctuating between distinct, long-lived functional states (19). Despite these advances, the nucleotide specificity of Ras bound to the active and allosteric sites of SOS and assembly with RAS, including oncogenic mutants, at the molecular level is poorly understood.

Targeting oncogenic Ras mutants presents significant challenges because of their relatively smooth surface that lacks potentially druggable pockets (6). Nevertheless, the discovery of KRas inhibitors, particularly those that form irreversible covalent bonds with Cys-12, comprises one of the most active areas of cancer research (6, 20). As there are few windows of opportunity to specifically target Ras mutants (6), apart from covalent binding to Cys-12, other approaches have also been explored, such as designing molecules to disrupt Ras•SOS interactions, thereby preventing activation of Ras (20). An increasing number of small-molecule disruptors and peptide mimetics have been designed to disrupt the Ras•SOS interaction (21). Potent small-molecule disruptors have recently been discovered that inhibit the formation of the Ras•SOS complex and demonstrate antiproliferative activity, representing a viable approach for targeting Ras-driven tumors (22, 23). These results highlight the therapeutic importance of disrupting the interaction between Ras and SOS.

Over the past three decades, native ion mobility–mass spectrometry (IM-MS) has evolved as a powerful analytical technique to investigate protein complexes and their interaction with other molecules (24–26). In native MS, biological samples in aqueous ammonium acetate are ionized using nanoelectrospray ionization and introduced into a mass spectrometer tuned to preserve noncovalent interactions and structure (24, 27). Native IM-MS can provide information on protein complexes, such as subunit stoichiometry and topology (28), and, unlike other biophysical

Significance

Disrupting the interaction between Ras and SOS has emerged as an attractive therapeutic strategy. Here, we characterized the assembly of the catalytic domain of SOS (SOS^{cat}) with oncogenic KRas mutants using native mass spectrometry. By resolving distinct molecular species, we show KRas mutants engage SOS^{cat} differently and the G13D KRas mutant robustly engages SOS^{cat}. A structure of $KRas^{G13D}$ in complex with SOS^{cat} shows repositioning of switch I and II regions within $KRas^{G13D}$. Moreover, potent small-molecule Ras•SOS disruptors do not dissociate $KRas^{G13D}$•SOS^{cat} complexes when $KRas^{G13D}$–GTP is bound at allosteric site of SOS^{cat}. These results underscore the need for more potent Ras•SOS disruptors when considering targeting the disruption of different oncogenic Ras mutants in complex with SOS.

Author contributions: Z.M., M.S., and A.L. designed research; Z.M., M.S., C.L., S.S., C.P., M.Z., and A.L. performed research; Z.M., C.L., C.P., D.H.R., M.Z., and A.L. analyzed data; and Z.M., M.S., S.S., C.P., D.H.R., M.Z., and A.L. wrote the paper.

The authors declare no competing interest.

This article is a PNAS Direct Submission.

[1]To whom correspondence may be addressed. Email: alaganowsky@chem.tamu.edu.

This article contains supporting information online at https://www.pnas.org/lookup/suppl/doi:10.1073/pnas.2022403118/-/DCSupplemental.

Published March 15, 2021.

techniques, resolve individual ligand-binding events (29). In combination with an apparatus to control temperature, native MS can be used to determine equilibrium binding constants and thermodynamics for protein–ligand and protein–protein that are in direct agreement with traditional biophysical approaches, such as isothermal calorimetry (30–35). Recently, native MS has been employed to determine transition state thermodynamics for the intrinsic GTPase activity of KRas and several oncogenic mutants (36). Notably, intrinsic GTPase activity rates determined using traditional solution-based assays mirrored those obtained using native MS (36).

Although the interaction of Ras and SOS has been the subject of numerous studies, the interaction of oncogenic Ras mutants with SOS remains poorly described. To better understand the role of these interactions in cancer, native IM-MS is used to characterize the molecular assemblies formed between SOS^{cat} and mutants of KRas associated with cancer. IM spectrometry shows conformational heterogeneity of SOS^{cat} with specific conformers engaging KRas. Three selected oncogenic mutants of KRas form distinct molecular assemblies with SOS^{cat}, such as $KRas^{G13D}$ forming exclusively a ternary complex with SOS^{cat}. The cryogenic electron microscopy (cryo-EM) structure of the $KRas^{G13D}$•SOS^{cat} complex provides insight into the mechanism for the higher affinity of $KRas^{G13D}$ for SOS^{cat}. $KRas^{G13D}$–GTP also allosterically modulates the activity of SOS^{cat} more than the wild-type protein. In addition, the recent inhibitors developed to disrupt the KRas•SOS^{cat} complex, BAY-293 and BI-3406, cannot dissociate $KRas^{G13D}$•SOS^{cat} complexes. Other small molecules, such as ARS-1620 and Kobee0065, display a range of efficacies in disrupting complexes formed between KRas mutants and SOS^{cat}.

Results

Conformational Dynamics of SOS^{cat} and Conformational Selection of KRas. To investigate the interaction between SOS and Ras, we selected SOS^{cat}, which can bind up to two Ras molecules, and KRas due to its importance in cancer (7, 8). The KRas•SOS^{cat} complex purified following methods established for structural studies (14, 15) was subjected to native IM-MS analysis, a biophysical technique that has recently monitored the intrinsic GTPase activity of KRas (36). The native mass spectrum of the purified complex revealed an equilibrium of molecular species (Fig. 1*A*). The KRas•SOS^{cat} complexes contained a nucleotide-free KRas and the ternary complex, KRas•SOS^{cat}•KRas–GTP–Mg^{2+} (active site•SOS^{cat}•allosteric site), composed of one KRas and KRas bound to GTP. Based on previous NMR and spectroscopic results showing the low affinity of KRas–GTP to the active site (15, 16), we presume KRas–GTP is bound to the allosteric site of SOS^{cat}. The stoichiometry of this ternary complex is consistent with crystal structures (14). Ion mobility measurements, which report on the rotationally averaged collision cross-section (CCS), show the existence of different conformers populated by SOS^{cat}, which could be modeled with a minimum of three different Gaussian distributions (Fig. 1*B* and *SI Appendix*, Fig. S1 and Table S1). A similar analysis of SOS^{cat} but in the absence of KRas (Fig. 1*C* and *SI Appendix*, Fig. S1) revealed a marked increase in the most compact conformers, which are depleted when KRas is present (Fig. 1*B*). The lack of SOS^{cat} repopulating these conformers in the presence of KRas is entirely consistent with the reported long-lived interconverting dynamical states of SOS^{cat} (18, 19). In another words, the observed depletion in SOS^{cat} conformers that preferentially engage KRas could only happen if the different conformers have slow interconverting rates and long-lived states, which do not repopulate or equilibrate on the timescale of the experiment, hence their observed depletion in abundance. These findings provide additional evidence of conformational dynamics of SOS^{cat} and conformational selection for binding KRas.

Molecular Assemblies of KRas–GTP and SOS^{cat}. To better understand the molecular assemblies of KRas with SOS^{cat} in the presence of unmodified nucleotides, we conducted studies using a higher-resolution mass spectrometer (29). We first mixed SOS^{cat} with a threefold molar excess of KRas loaded with GTP (KRas–GTP) (*SI Appendix*, Fig. S2). The mass spectrum recorded immediately after mixing shows the presence of monomeric and dimeric KRas bound to GTP, and a single binary complex composed of SOS^{cat}•KRas–GTP–Mg^{2+} (Fig. 1 *D* and *I*). In addition, two ternary complexes of near equal abundance were measured corresponding to KRas•SOS^{cat}•KRas–GTP–$Mg^{2+}(GDP)_{0–1}$ (Fig. 1*E*). The measured molecular weight of these complexes and of the proteins alone are in good agreement with theoretical values (*SI Appendix*, Table S2). Notably, these molecular species were not resolved in

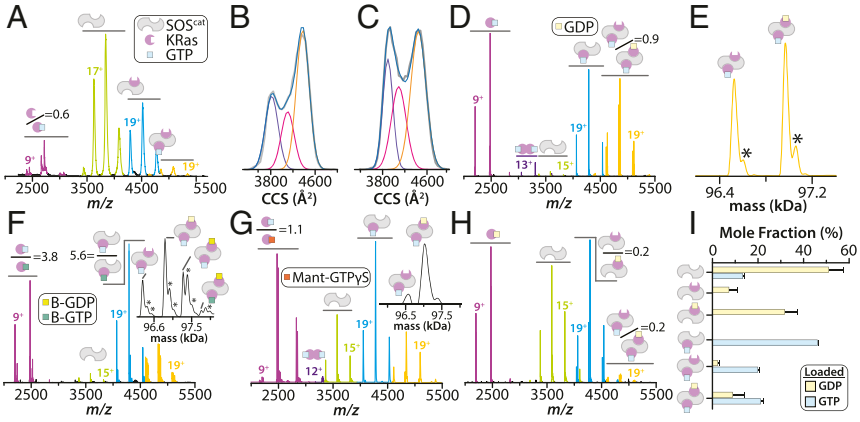

Fig. 1. Conformational dynamics and molecular assemblies of SOS^{cat} and KRas. (*A*) Native mass spectrum of 2 μM KRas•SOS^{cat} complex purified by size exclusion chromatography. Mass spectral peaks corresponding to KRas, SOS^{cat}, binary, and ternary complexes are colored purple, chartreuse, cyan, and orange, respectively. (*B*) Collision cross-section (CCS) distribution for the 16^+ ion of SOS^{cat} (blue lines). Regression ($R^2 = 1.0$) of three Gaussian peaks (purple, pink, and orange lines) and their sum (gray line). (*C*) CCS profile for the 16^+ ion of SOS^{cat} recorded in the absence of KRas. Shown as described in *B*. (*D*) Mass spectrum of 2 μM SOS^{cat} and 6 μM KRas–GTP recorded immediately after mixing. (*E*) Deconvolution of mass spectrum in *D* and selected mass range corresponding to ternary complexes. Inorganic phosphate adducts are denoted by an asterisk. (*F* and *G*) Mass spectrum for the mixture described in *D* with the addition of (*F*) 2 μM BODIPY modified GTP (B-GTP) and (*G*) 5 μM Mant-GTPγS. (*H*) Mass spectrum of 2 μM SOS^{cat} and 6 μM KRas–GDP recorded immediately after mixing. (*I*) Plot of the mole fraction of SOS^{cat} complexes determined from deconvolution of mass spectra. Reported are the mean and SD ($n = 3$). Mass spectra shown in *D*–*H* were acquired on an Exactive plus EMR Orbitrap mass analyzer. KRas bound at active and allosteric sites are shown at *Top Right* and *Bottom Left* of the cartoon, respectively.

the lower-resolution mass spectrum (Fig. 1*A*). KRas bound to GTP dominates the binary and ternary complexes, a result that is consistent with the higher affinity of KRas–GTP to the allosteric site (15, 16). These findings capture an equilibrium of molecular assemblies formed between KRas and SOS^{cat} that would be difficult to render using other biophysical techniques.

SOS^{cat} Stimulates KRas GTPase Activity. Despite addition of KRas–GTP to SOS^{cat}, an additional peak corresponding to KRas•SOS^{cat} •KRas–GTP–Mg^{2+}(GDP)$_1$ was detected with a measured mass (96,972.2 ± 2.3 Da) in close agreement with the calculated mass (96,964.8 Da) (*SI Appendix*, Table S2). Mass selection of this ternary complex in the quadrupole followed by collision-induced dissociation (CID) further corroborates this assignment (*SI Appendix*, Fig. S3). In addition, surface-induced dissociation (SID) of the isolated ternary complex resulted in dissociation of KRas and KRas–GTP from the complex (*SI Appendix*, Fig. S4). Notably, KRas was loaded with GTP (~98%) (*SI Appendix*, Fig. S2) and the slow intrinsic GTP hydrolysis of KRas in the absence of SOS^{cat} cannot account for the perplexing abundance of GDP. The appearance of GDP is most likely due to the GTPase activity of KRas but stimulated by SOS^{cat}, which would result in production of GDP and inorganic phosphate ($H_2PO_4^-$). In crystal structures (14), phosphate is bound to ternary complexes, and accordingly here phosphate adducts are observed on the complex with a measured mass of 97,060.2 ± 2.1 Da compared to the theoretical mass of 97,061.8 Da (Fig. 1*E*). Moreover, incubation of a mixture of KRas–GTP and SOS^{cat} overnight resulted in nearly twofold greater levels of KRas bound to GDP compared to the control solution containing only KRas–GTP (*SI Appendix*, Fig. S5). An inorganic phosphate assay also corroborated these findings with higher phosphate concentration when KRas–GTP is in the presence of SOS^{cat} compared to the control KRas–GTP solution (*SI Appendix*, Table S3). Taken together, these results indicate a role of SOS in stimulating the GTPase activity of KRas.

Additional evidence for stimulation of KRas GTPase activity is offered by the use of GTP analogs. First, a BODIPY-modified GTP (B-GTP) analog was added to an incubated mixture of KRas–GTP and SOS^{cat} followed by recording the native mass spectrum. Multiple species are observed along with adducts corresponding to inorganic phosphate and B-GDP only bound to KRas in complex with SOS^{cat} (Fig. 1*F*). Interestingly, the lower abundance of KRas•SOS^{cat} •KRas–B-GTP·Mg^{2+}(B-GDP)$_1$ compared to KRas•SOS^{cat} •KRas–GTP–Mg^{2+}(B-GDP)$_1$ suggests the allosteric binding site is less dynamic than the active site (Fig. 1 *F*, *Inset*). Next, the nonhydrolyzable GTP analog, Mant-GTPγS, was added to the incubated mixture of SOS^{cat} and KRas–GTP. The native mass spectrum shows no detectable signal corresponding to hydrolyzed Mant-GDP, and Mant-GTPγS is only bound to free KRas (Fig. 1*G*). These findings show various molecular assemblies of KRas and SOS^{cat} but also report that SOS^{cat} can stimulate of KRas GTPase activity, a characteristic feature of GTPase-activating proteins (GAPs) (4).

Molecular Assemblies of KRas–GDP and SOS^{cat}. As the degree of allosteric modulation of SOS^{cat} greatly depends on the nucleotide-bound state of Ras (14, 16), KRas was loaded with GDP (KRas–GDP) prior to mixing with SOS^{cat}. The native mass spectrum for this mixture is dominated by two binary complexes with the majority (~80%) bound to GDP (Fig. 1 *H* and *I*). In addition, there are low abundant signals corresponding to KRas•SOS^{cat} •KRas–GTP–Mg^{2+}(GDP)$_{0–1}$ that stem from a small fraction of KRas–GTP not loaded with GDP (*SI Appendix*, Fig. S6), underscoring the sensitivity of our measurements. KRas–GTP promotes the formation of a ternary complex, which is in accord with previous studies (14, 16).

Molecular Assemblies of SOS^{cat} and KRas Oncogenic Mutants. Three oncogenic mutants of KRas were selected based on their high occurrence in some cancers (Q61H, G13D, and G12C) (5). The mutant proteins were first loaded with GTP and mixed with SOS^{cat} immediately before native MS analysis. The mass spectrum for KRas^{Q61H} and SOS^{cat} mixture showed a higher abundance of dimeric KRas^{Q61H} with each bound to GTP and no detectable ternary complex (Fig. 2 *A* and *D*). The SOS^{cat}•KRas^{Q61H}–GTP–Mg^{2+} complex uniformly contained one GTP and no ternary complexes were observed (Fig. 2 *A* and *D*). In stark contrast, KRas^{G13D}–GTP solely formed a KRas^{G13D}•SOS^{cat} •KRas^{G13D}–GTP–Mg^{2+} complex (Fig. 2 *B* and *D*). The third GTP-loaded mutant KRas^{G12C} engaged SOS^{cat} in a similar fashion as wild-type KRas with the exception of an increased abundance of the ternary complex containing GDP (Fig. 2 *C* and *D* and *SI Appendix*, Fig. S7). Of the three oncogenic mutants, GDP was observed only in SOS^{cat}•KRas^{G12C} complexes. In summary, oncogenic mutants form assemblies with SOS^{cat} that are distinct from those formed with wild-type KRas.

We next investigated the three oncogenic mutants loaded with GDP and their assembly with SOS^{cat}. The mass spectrum of a 3:1 mixture of KRas^{Q61H} to SOS^{cat} had weak signal for a GDP-bound binary complex (Fig. 2 *E* and *H*). KRas^{G13D}–GDP predominantly formed ternary complexes composed of KRas^{G13D}•SOS^{cat}•KRas^{G13D}–GDP(GDP)$_{0–1}$ with ~90% of the signal accounting for the complex bound to only

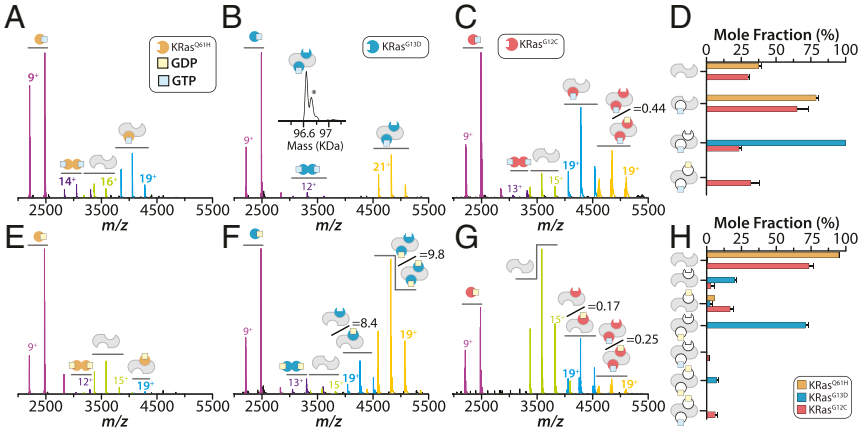

Fig. 2. Distinct molecular assemblies of SOS^{cat} with oncogenic KRas mutants. (*A–C*) Native mass spectra of 2 μM SOS^{cat} mixed with three equivalents of (*A*) KRas^{Q61H}–GTP, (*B*) KRas^{G13D}–GTP, or (*C*) KRas^{G12C}–GTP. Mass spectra are shown as described in Fig. 1. (*D*) Plot of the mole fraction of SOS^{cat} complexes formed with GTP-loaded proteins. (*E–G*) Mass spectra of 2 μM SOS^{cat} mixed with threefold molar excess of (*E*) KRas^{Q61H}–GDP, (*F*) KRas^{G13D}–GDP, or (*G*) KRas^{G12C}–GDP. (*H*) Plot of the mole fraction of SOS^{cat} complexes formed with GDP-loaded proteins. Shown as described in Fig. 1.

one GDP (Fig. 2 *F* and *H*). This unexpected observation of a prevalent ternary complex for $KRas^{G13D}$–GDP suggests it can bind the allosteric site and possibly function as an allosteric modulator of SOS^{cat}. Assembly of SOS^{cat} and $KRas^{G12C}$–GDP led to the formation of complexes reminiscent of wild-type KRas but overall lower in abundance (Fig. 2 *G* and *H*).

Complexes of KRas with a Mutant Form of SOS^{cat}. SOS^{cat} containing the W729E mutation (SOS^{W729E}) has been reported to abolish Ras binding at the allosteric site (15). The mixture of KRas–GTP and SOS^{W729E} showed a significant depletion of higher-order complexes (Fig. 3 *A* and *C*). Again, GDP is present in the ternary complex with a ratio skewed to those containing GDP. $KRas^{Q61H}$–GTP and $KRas^{G12C}$–GTP also displayed an overall reduction in complex formation (Fig. 3*C* and *SI Appendix*, Fig. S8). Surprisingly, $KRas^{G13D}$–GTP formed complexes composed of $KRas^{G13D}$•SOS^{W729E} and $KRas^{G13D}$•SOS^{W729E}•$KRas^{G13D}$–GTP–Mg^{2+} (Fig. 3 *B* and *C*). Moreover, SOS^{W729E} and KRas–GDP formed two binary complexes, KRas•$SOS^{W729E}$$(GDP)_{0–1}$, in the same ratio but lower in signal abundance compared to SOS^{cat} alone (Fig. 3 *D* and *F*). $KRas^{G13D}$–GDP primarily assembled into binary complexes with a majority (~64%) containing nucleotide-free $KRas^{G13D}$ (Fig. 3 *E* and *F*). $KRas^{G12C}$•$SOS^{W729E}$$(GDP)_{0–1}$ complexes were observed for the assembly of $KRas^{G12C}$–GDP and SOS^{W729E}, and $KRas^{Q61H}$–GDP did not engage SOS^{W729E} (Fig. 3*F* and *SI Appendix*, Fig. S8). Taken together, these results demonstrate a clear preference for the active site of SOS^{cat} toward KRas–GDP.

Structural Characterization of the $KRas^{G13D}$–GTP and SOS^{cat} Ternary Complex. The unique properties of $KRas^{G13D}$ to form predominantly ternary complexes with SOS^{cat} prompted us to determine the structure using cryo-EM. The ternary complex was prepared using $KRas^{G13D}$ loaded with 5′-guanylyl imidodiphosphate (GppNp), a nonhydrolyzable analog of GTP (*SI Appendix*, Fig. S9). The structure of the complex was determined to a resolution of 3.47 Å (*SI Appendix*, *Methods*) with $KRas^{G13D}$ and $KRas^{G13D}$–GTP bound at the active and allosteric sites of SOS^{cat}, respectively (Fig. 4*A* and *SI Appendix*, Fig. S10). The presence of nucleotide-free $KRas^{G13D}$ at the active site is in line with MS results (Fig. 2*B*). The structure is largely reminiscent with that of HRas•SOS^{cat}•HRas–GppNp (Protein Data Bank [PDB] 1NVW) with some notable structural differences, such as a ~2.5-Å displacement of the $KRas^{G13D}$ molecule at the active site (*SI Appendix*, Fig. S11 *E* and *F*). Analysis of $KRas^{G13D}$–GTP bound at the allosteric site reveals that $KRas^{G13D}$ adopts a state 2 conformation, characterized by interaction of the γ-phosphate with the side chain of Thr35 within switch I and the amide of Gly60 within switch II (*SI Appendix*, Fig. S11*B*) (37). Moreover, the structure of $KRas^{G13D}$–GppNp bound at the allosteric site of SOS^{cat} aligns well with that of active conformation of HRas–GTP (*SI Appendix*, Fig. S11*C*) (37). However, the molecular interactions of $KRas^{G13D}$–GTP bound at the allosteric site of SOS^{cat} differs from that observed for SOS^{cat} in complex with HRas–GTP. More specifically, the side chain of tryptophan at position 729 of SOS^{cat} is reoriented and interacting with the carbonyl of Pro34 of $KRas^{G13D}$ (Fig. 4 *A* and *B*). The orientation of Trp729 is similar to the crystal structure of the Tyr64Ala mutant of HRas bound at the allosteric site of SOS^{cat} (*SI Appendix*, Fig. S11*D*), which this mutant HRas protein has significantly reduced binding affinity to the active site of SOS^{cat} (38). Trp729 adopts a different orientation that interacts with Try64 in the structure of HRas–GppNp bound at the allosteric site of SOS^{cat} (Fig. 4*C*). The density for residues 62–67 within the switch II region was not clear, possibly due to this region populating different conformations. The most marked difference in the structure of the $KRas^{G13D}$ in complex with SOS^{cat} compared to other available structures (14, 22) is the structure of $KRas^{G13D}$ bound at the active site (Fig. 4*D*). Aspartic acid at position 13 forms hydrogen bonds with Asn86 and Lys117. These interactions, for example, reposition loop 8 by ~4 Å compared to HRas in complex with SOS^{cat} along with displacing other regions, such as helices 3 and 4, p-loop, and switch I (Fig. 4*D* and *SI Appendix*, Fig. S11*E*). The observed conformation of $KRas^{G13D}$ also differs from the structure of a mutated form of $KRas^{G12C}$ bound only at the active site of SOS^{cat} (*SI Appendix*, Fig. S11*F*). Comparison of the $KRas^{G13D}$–GDP structure (PDB 6E6G) with $KRas^{G13D}$ bound at the active site reveals the side chain of Asp13 is rotated 180° and pointing away from Asn86 (Fig. 4*E*).

The Modulation of SOS^{cat} Activity by $KRas^{G13D}$–GTP. Competition and nucleotide exchange assays were conducted to better understand the significance of the interaction between $KRas^{G13D}$ and SOS^{cat}. First, the complex formed between SOS^{cat} with GTP-loaded KRas harboring the N-terminal hexahistidine affinity tag (His_6–KRas–

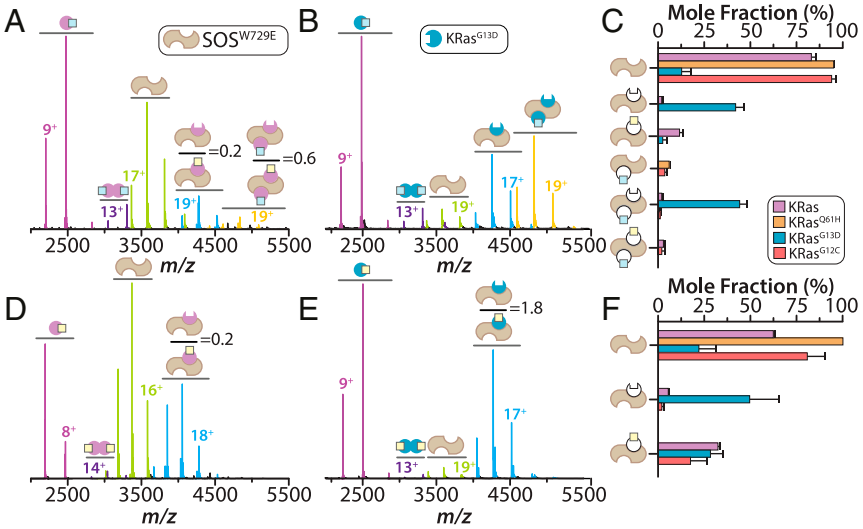

Fig. 3. Complexes of a mutant form of SOS^{cat} with KRas and oncogenic mutants. (*A* and *B*) Native mass spectra of 2 μM SOS^{W729E} mixed with 6 μM of (*A*) KRas–GTP or (*B*) $KRas^{G13D}$–GTP. Mass spectra are shown as described in Fig. 1. (*C*) Plot of the mole fraction of SOS^{W729E} complexes formed with GTP-loaded proteins. Shown as described in Fig. 1. (*D* and *E*) Mass spectra for a 1:3 mixture of SOS^{W729E} with (*D*) KRas–GDP or (*E*) $KRas^{G13D}$–GDP. (*F*) Plot of the mole fraction of SOS^{W729E} complexes formed with GDP-loaded proteins. Shown as described in Fig. 1.

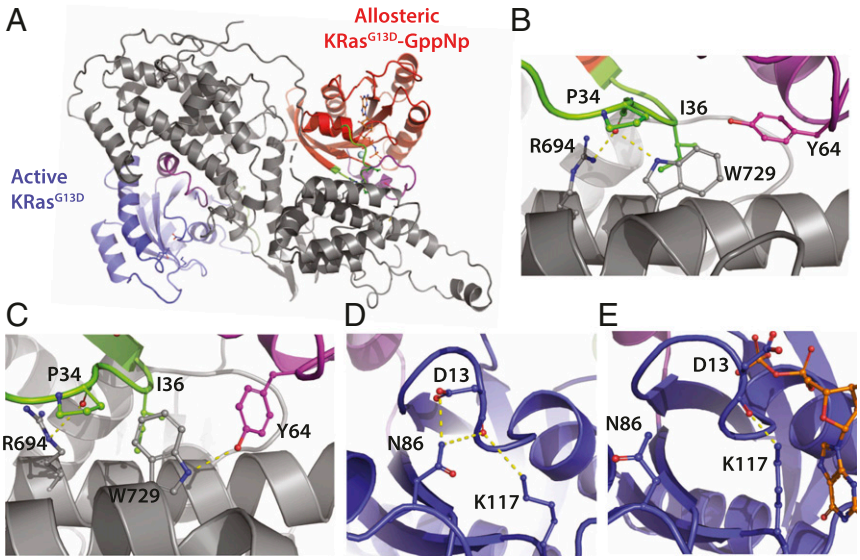

Fig. 4. Structure of KRas^{G13D} in complex with SOS^{cat}. (*A*) The structure is shown in cartoon representation with KRas^{G13D} molecules bound at the active and allosteric sites of SOS^{cat} (gray), which are colored blue and red, respectively. Switch I and II regions of KRas^{G13D} are colored in green and purple, respectively. Allosteric KRas^{G13D} is bound to GppNp and magnesium. (*B*) Molecular interactions formed at the interface between KRas^{G13D}–GppNp and SOS^{cat}. Hydrogen bonds are shown as yellow dashed lines. (*C*) The allosteric interface for HRas–GppNp and SOS^{cat} (PDB 1NVW) (14) shown in similar orientation as *B*. (*D*) KRas^{G13D} bound at the active site with Asp13 forming interactions with Asn86 and K117. (*E*) X-ray structure of KRas^{G13D} bound to GDP (PDB 6E6G) (51) shows the side chain of Asp13 is oriented in the opposite direction, away from Asn86.

GTP) displayed similar abundances of molecular species as the tagless protein (Fig. 5*A*). Interestingly, addition of KRas^{G13D}–GTP to this complex not only completely abolished the binding of wild-type KRas to SOS^{cat} but predominantly formed a ternary complex of KRas^{G13D}•SOS^{cat} •KRas^{G13D}–GTP–Mg^{2+} (Fig. 5*B*). The experiment performed in the opposite fashion, where His_6–KRas–GTP is added to preformed complexes of KRas^{G13D}–GTP and SOS^{cat}, resulted in no disruption of KRas^{G13D}•SOS^{cat} complexes (*SI Appendix*, Fig. S12). Next, the SOS^{cat}-stimulated nucleotide exchange rate of KRas bound to B-GDP in the absence and presence of KRas^{G13D}–GTP was determined. The intrinsic nucleotide exchange rate of KRas–B-GDP is slow (39) ($k = 0.12$ min^{-1}) but enhanced in the presence of SOS^{cat} (Fig. 5*C*). The rate of nucleotide exchange is allosterically modulated ($k = 0.3$ min^{-1}) in the presence of KRas–GTP (Fig. 5 *C* and *D*) consistent with previous studies (14). However, the addition of KRas^{G13D}–GTP increased the exchange rate by more than twofold, $k = 0.7$ min^{-1} (Fig. 5 *C* and *D*). The addition of KRas^{Q61H}–GTP ($k = 0.4$ min^{-1}) marginally increased the nucleotide exchange rate compared to KRas–GTP and much less than KRas^{G13D}–GTP. Attempts to measure SOS^{cat}-mediated nucleotide exchange rate of KRas^{G13D} in the presence of allosteric KRas^{G13D}–GTP was not possible due to extremely fast nucleotide exchange rate of this mutant protein consistent with previous studies (17). In short, KRas^{G13D} exhibits not only a higher affinity for SOS^{cat} but is also a more potent allosteric modulator of SOS^{cat} activity.

Disruption of the Interaction between KRas and SOS^{cat}. As the disruption of the interaction between Ras and SOS is an attractive approach to curb aberrant Ras signaling (21, 40), we next investigated whether small-molecule Ras•SOS disruptors can efficiently disrupt complexes of SOS^{cat} and KRas mutants. Recent traction has been made on the development of specific covalent inhibitors of KRas^{G12C}, such as ARS-1620 (20, 41). Reacting 10 equivalents of ARS-1620 with KRas^{G12C} loaded with either GTP or GDP showed complete reactivity when the enzyme is bound to GDP and limited reactivity when GTP is bound (*SI Appendix*, Fig. S13). These results agree with the specificity of ARS-1620 toward the inactive, GDP-bound state of KRas^{G12C}. Moreover, the addition of ARS-1620 to an incubated mixture of SOS^{cat} and KRas^{G12C}–GDP resulted in complete disruption of complexes (Fig. 6*A*), consistent with a SOS-mediated nucleotide exchange assay (41). However, ARS-1620 added to a preincubated mixture of SOS^{cat} and KRas^{G12C}–GTP had no appreciable disruption of binary and ternary complexes (Fig. 6*E*). This result suggests KRas^{G12C}–GTP allosterically modulates the affinity of KRas^{G12C} at the active site of SOS^{cat}, thereby hindering the reactivity of ARS-1620. These findings highlight the inability of ARS-1620 to disrupt assemblies of SOS^{cat} and KRas^{G12C}–GTP.

We next tested the efficacy of small-molecule Ras•SOS disruptors, Kobe0065 ($IC_{50} = 20$ μM), BAY-293 ($IC_{50} = 21$ nM), and BI-3406 ($IC_{50} = 5$ nM) (22, 23, 42). Kobe0065 binds directly to Ras–GTP and is reported to alter the binding at the allosteric site of SOS (42). The addition of 2.5 equivalents of Kobe0065 to SOS^{cat} in complex with KRas–GTP or KRas^{G13D}–GTP resulted in marginal and no disruption, respectively (Fig. 6 *B* and *F*). Increasing the concentration of Kobe0065 to 200 μM, 10 times the reported IC_{50} value, did not disrupt binary and ternary complexes. In addition, the small molecule was ineffective at disrupting complexes of KRas^{G12C} and SOS^{cat} (*SI Appendix*, Fig. S14*C*). BAY-293 has been shown to efficiently disrupt the interaction between KRas^{G12C} and SOS^{cat} leading to antiproliferative activity (22). However, the small molecule was not effective at disrupting the binding of KRas–GTP and KRas^{G12C}–GTP at the allosteric site of SOS^{cat} (Fig. 6*C* and *SI Appendix*, Fig. S14*B*). BAY-293 binds directly to SOS^{cat} (*SI Appendix*, Fig. S14*A*) and disrupts the ternary complexes formed between SOS^{cat} and KRas or KRas^{G12C} (Fig. 6*C* and *SI Appendix*, Fig. S14*B*). Moreover, BAY-293 did not disrupt the ternary complex of KRas^{G13D}–GTP and SOS^{cat} (Fig. 6*G*). The compound, however, does inhibit the formation of complexes formed between SOS^{W729E} and either KRas–GDP or KRas^{G13D}–GDP (*SI Appendix*, Fig. S14 *D* and *E*). BI-3406 (23), a recently reported highly selective and potent inhibitor of SOS1, was screened for the ability to disrupt complexes formed between SOS^{cat} and wild-type and mutants of KRas. At 2.5 μM, BI-3406 binds directly to SOS^{cat} (*SI Appendix*, Fig. S15*A*) and disrupts the ternary complex between SOS^{cat} and KRas (Fig. 6*D*). In contrast,

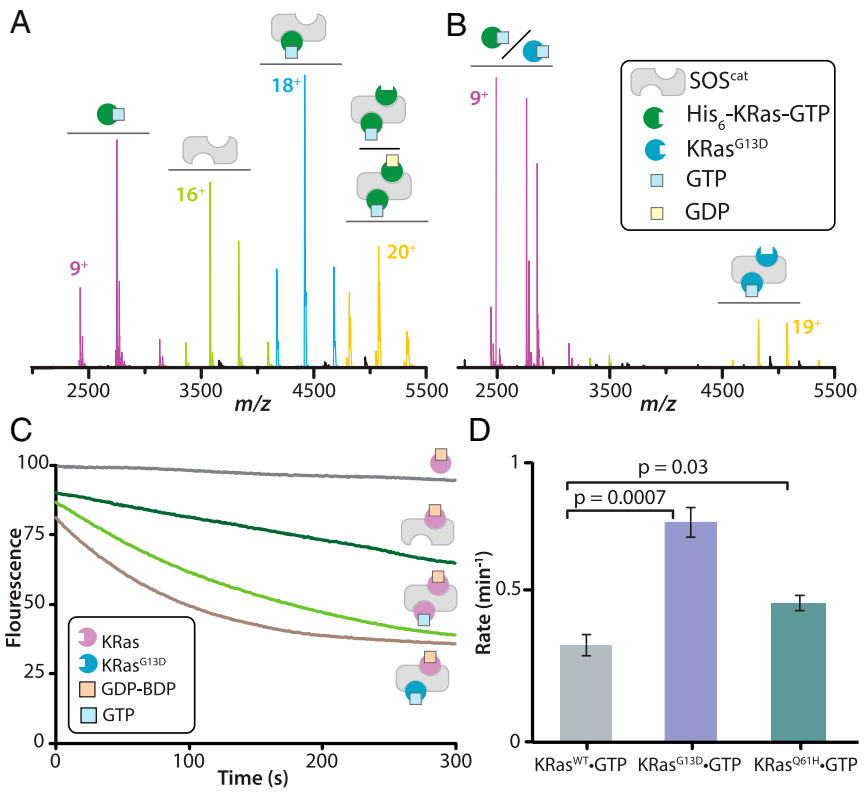

Fig. 5. Competition and cross-activation of $KRas^{G13D}$–GTP. (*A*) Native mass spectrum of 1 μM SOS^{cat} in complex with 3 μM His_6–KRas–GTP. (*B*) Native mass spectrum after adding $KRas^{G13D}$–GTP to the mixture in *A* to a final concentration of 3 μM. Mass spectra are shown as described in Fig. 1. (*C*) Intrinsic (black line) and SOS^{cat}-mediated (dark green line) nucleotide exchange of KRas loaded with B-GDP. The addition of KRas–GTP (light green line) or $KRas^{G13D}$–GTP (brown line) to a mixture of KRas–B-GDP and SOS^{cat} accelerates the nucleotide exchange rate. (*D*) Nucleotide exchange rates determined for data presented in *C*. The SOS^{cat}-mediated nucleotide exchange rate in the presence of $KRas^{Q61H}$–GTP is also provided. Reported are the mean and SD from three independent experiments.

BI-3406 at the same concentration did not disrupt the ternary $KRas^{G13D}$•SOS^{cat} complex (Fig. 6*H*), even after overnight incubation (*SI Appendix*, Fig. S15*B*). At higher concentrations of the compound (4,000-fold the reported IC_{50}), the ternary complex between $KRas^{G13D}$ and SOS^{cat} was almost completely disrupted (*SI Appendix*, Fig. S15*C*). Similar to BAY-293, BI-3406 disrupts the binary complex between $KRas^{G13D}$–GDP and SOS^{W729E} (*SI Appendix*, Fig. S15*D*).

Discussion

Dynamics of signaling proteins play crucial roles in their function (43). Although conformational heterogeneity has been reported for SOS^{cat} (18, 19), ion mobility measurements provide direct experimental evidence of the protein populating at least three conformers in solution with distinct conformers engaging KRas. If the dynamics were fast, the depleted conformers that engage with KRas would be repopulated. Instead, depletion of specific conformers in the presence of KRas is in direct agreement with the long-lived, interconverting dynamical nature of SOS^{cat} (18, 19). This is a demonstration of ion mobility showing clear evidence of conformational selection for a protein–protein interaction.

Native MS provides a unique opportunity to monitor the molecular assemblies of SOS^{cat} with Ras. Unlike other approaches, the sensitivity and resolution of modern mass spectrometers enable not only measurements of proteins at low micromolar concentration but use of unmodified nucleotides. Native mass spectra resolve a number of molecular assemblies formed between KRas and SOS^{cat} that populate different nucleotide-bound states. The abundances of various nucleotide-bound states of binary and ternary complexes provide a glimpse into the affinity of nucleotides. For example, binary and ternary complexes of $KRas^{G13D}$ are dominated by nucleotide-free states that may have bearing to the reported fast nucleotide exchange rates of the mutant protein (39). We also find an unexpected abundance of GDP immediately after mixing KRas–GTP with SOS^{cat}, and addition of B-GTP to preformed ternary complex further validates the SOS^{cat}-mediated stimulation of KRas GTPase activity. However, no GDP was observed when a nonhydrolyzable analog is added to the complex. The presence of GDP was also observed for $KRas^{G12C}$, which has reduced intrinsic GTPase activity compared to the wild-type protein (36). These results provide compelling evidence that SOS^{cat} has GAP-like characteristics. Nevertheless, it is unknown whether the hydrolysis reaction is carried out at the active or allosteric site(s) of SOS^{cat}. The observed ions corresponding to KRas•$SOS^{W729E}(GDP)_1$ after immediate MS analysis of a KRas–GTP and SOS^{W729E} mixtures suggests that the hydrolysis reaction likely occurs at the active site. Furthermore, SOS^{W729E} engineered to disrupt binding at the distal site shows a clear preference for binding KRas–GDP at the active site, consistent with previous reports (15–17). However, our data also show SOS^{W729E} does not completely abolish binding at the distal site as reported (15), thereby convoluting the interpretation of reported binding affinities (15–17). In addition, signal is detected corresponding to dimers of wild type and oncogenic mutants of KRas. At the concentration of KRas (3 μM) used in the native MS studies, it is unlikely that the homodimers arise from nonspecific association and provide direct evidence of KRas dimerization, which has been implicated in Ras signaling (44).

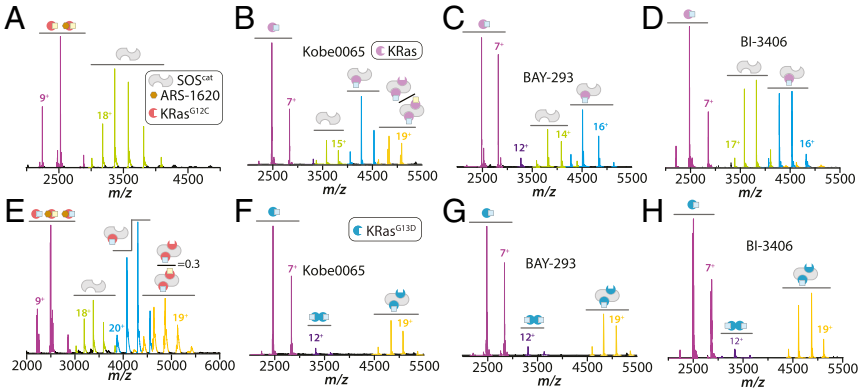

Fig. 6. The effect of ARS-1620, BAY-293, and Kobe0065 on assemblies of KRas and SOS^{cat}. (*A–E*) Mass spectrum recorded after adding 10 μM ARS-1620 to preincubated mixtures of 1 μM SOS^{cat} with 3 μM (*A*) KRas^{G12C}–GDP and (*E*) KRAS^{G12C}–GTP. Mass spectra are shown as described in Fig. 1. (*B–F*) Mass spectrum recorded after adding 2.5 μM Kobe0065 to preincubated mixtures of 1 μM SOS^{cat} with 3 μM (*B*) KRas–GTP and (*F*) KRAS^{G13D}–GTP (*C–G*) Mass spectrum recorded after adding 2.5 μM BAY-293 to preincubated mixtures of 1 μM SOS^{cat} with 3 μM (*C*) KRas–GTP and (*G*) KRAS^{G13D}–GTP. (*D–H*) Mass spectrum recorded after adding 2.5 μM BI-3406 to preincubated mixtures of 1 μM SOS^{cat} with 3 μM (*D*) KRas–GTP and (*H*) KRAS^{G13D}–GTP.

The structure of KRas^{G13D}•SOS^{cat}•KRas^{G13D}–GppNp provides molecular details and clues to understanding the observed higher binding affinity of KRas^{G13D} for SOS^{cat}. First, KRas^{G13D} bound at the active site of SOS^{cat} is displaced compared to those in complex with HRas and KRas^{G12C} (14, 22). Asp13 forms molecular interactions that reorients its side chain away from the nucleotide binding pocket that is essentially primed for binding GTP to a greater extent than the wild-type protein. This observation draws a corollary to native MS results, where the majority of the ternary complex is not bound to GDP. Aside from structural differences observed at the active site, the overall structural similarity to the HRas•SOS^{cat}•HRas–GppNp complex indicate the molecular interactions would be similar for HRas, KRas, and KRas^{G13D}. Therefore, a plausible explanation for the observed higher binding affinity of KRas^{G13D} is likely due to the altered dynamics of the mutant protein. In particular, switch II of KRas^{G13D} is known to become less flexible, regardless of nucleotide-bound state, and positively correlated with β2–β3 loop motions (45). Importantly, switch II forms key interactions at the allosteric site of SOS^{cat}, and the altered dynamics of switch II in KRas^{G13D} could result in an increase in the apparent binding affinity, i.e., a larger fraction of KRas^{G13D} adopts a conformation(s) that can selectively engage SOS^{cat}. Moreover, the reduced dynamics of the switch II region of the KRas^{G13D}–GDP can partly explain the ability of the GDP-bound protein to bind at the allosteric site and form ternary complexes with SOS^{cat}.

As oncogenic mutants have impaired GTPase activity, it has been surmised that activation of oncogenic Ras is independent of SOS (46). For example, activation of KRas^{G13D} and KRas^{Q61H} has been suggested to be independent of SOS due to their fast nucleotide exchange rate and impaired-GTPase activity, respectively (17, 39). However, results from native MS reveal KRas oncogenic mutants show an assortment of molecular assemblies ranging from weakly interacting KRas^{Q61H} to KRas^{G13D} that robustly engages SOS^{cat}. More specifically, KRas^{Q61H}–GTP does not exert an allosteric effect implying that activation of this mutant is likely SOS independent. In contrast, KRas^{G13D}–GTP unexpectedly forms predominantly a KRas^{G13D}•SOS^{cat}•KRas^{G13D}–GTP complex. KRas^{G13D}–GDP also forms KRas^{G13D}•SOS^{cat} •KRas^{G13D}–GDP(GDP)$_{0–1}$ complexes, suggesting the GDP-bound form of this mutant may serve as an allosteric modulator of SOS^{cat}. Moreover, KRas^{G13D}–GTP is a potent allosteric modulator of SOS^{cat} and can also enhance the SOS-mediated nucleotide exchange of wild-type KRas. Considering cancer cells can be heterozygous for the KRas^{G13D} mutation, these findings are of particular importance as SOS activity can be allosterically modulated by KRas^{G13D}, regardless of nucleotide-bound state, which in turn would lead to robust SOS-mediated activation of KRas. These findings provide additional evidence that oncogenic Ras bound at the allosteric site of SOS can cross-activate KRas, which has been shown to be essential for tumorigenesis (47).

Ras activation is tightly regulated by SOS and disruption of this interaction is an attractive route for targeting Ras-driven cancers (21, 40). ARS-1620 (IC_{50}, 120 nM) cannot disrupt assemblies of SOS^{cat} and KRas^{G12C}–GTP, suggesting KRas^{G12C}–GDP within the ternary complex is shielded from reaction with ARS-1620. KRas^{G12C}–GTP allosterically promotes the interaction of KRas^{G12C} at the active site, which diminishes the efficacy of the inhibitor to dissociate the complex. Kobe0065, designed to disrupt Ras binding at the allosteric site of SOS^{cat}, was ineffective for complexes formed with KRas, KRas^{G12C}, and KRas^{G13D}. The recent discovery of KRas•SOS disruptors have shown promising antiproliferative activity (22, 23). However, we show that while BAY-293 successfully disrupts KRas and KRas^{G12C} complexes with SOS^{cat}, it fails to disrupt those formed with KRas^{G13D} at 119-fold the IC_{50} (IC_{50} = 21 nM). Addition of BI-3406, 500-fold above the IC_{50} (IC_{50} = 5nM), did not disrupt the ternary complex of KRas^{G13D}–GTP and SOS^{cat}. Although BAY-293 and BI-3406 compounds can disrupt KRas^{G13D} binding to the active site of SOS^{cat} (*SI Appendix*, Figs. S14*E* and S15*D*), the presence of KRas^{G13D}–GTP bound at the allosteric site of SOS^{cat} leads to enhanced stability of the ternary complex that is persistent to disruption with these small-molecule disruptors. The antitumor activity of BAY-293 and BI-3406 is greatly enhanced in combination with specific KRas^{G12C} and MEK1 inhibitors (22, 23), and this strategy may mitigate cases where the efficacy of small-molecule Ras•SOS disruptors is reduced when SOS is engaged with oncogenic Ras mutants, such as KRas^{G13D}. Overall, the ability of KRas^{G13D} to exclusively form ternary complexes with SOS^{cat}, compete with KRas binding SOS^{cat}, activate SOS^{cat} to facilitate loading of wild-type KRas, and resistance to disruption by small-molecule disruptors may explain the aggressive biology of tumors associated with this mutant (48). Moreover, the higher binding affinity of KRas^{G13D}, and likely other Ras mutants, for SOS may lead to not only an increase in the recruitment of SOS to the plasma membrane but also prolong dwell time allowing an increase in Ras activation by SOS (49). In closing, these results showcase the ability of native IM-MS to provide unprecedented insight into molecular assemblies, such as those formed between SOS^{cat} and KRas, and open avenues to develop more potent Ras-SOS inhibitors, especially for Ras mutants that robustly bind and activate SOS.

Methods

Protein Expression and Purification. Human KRas4B (residues 1–169) and SOS^{cat} (residues 558–1049) were expressed and purified as previously described (36). The details of expression and purification are in *SI Appendix, Materials and Methods*. All mutations were generated using the Q5 site-directed mutagenesis kit (New England Biolabs) following the manufacturer's protocol. Additional details are in *SI Appendix, Materials and Methods*.

Sample Preparation to Monitor the Assembly of the Complex via Native MS Analysis. In order to obtain mass spectra of KRas or mutants (loaded with GDP or GTP) complexed with SOS^{cat} or SOS^{W729E}, KRas, SOS^{cat}, and SOS^{W729E} were separately buffer exchanged into 100 mM ammonium acetate (pH 7.4) using a Micro BioSpin 6 column (Bio-Rad). The GTP- or GDP-loaded KRas was mixed with SOS^{cat} or SOS^{W729E} at 3:1 molar ratio in ammonium acetate and immediately analyzed using native MS. For BODIPY-GTP and Mant-GTPγS experiments, 2 and 5 μM of the fluorophore analogs were added to the preformed mixture of SOS^{cat} and KRas–GTP, respectively (Fig. 1*D*), and were immediately analyzed using native MS. Additional details are available in *SI Appendix, Materials and Methods* for inhibitor binding assays.

Native MS. Protein samples were introduced into an Exactive Plus with extended mass range (EMR) Orbitrap MS (Thermo Fisher Scientific). Samples were loaded into pulled borosilicate glass capillaries prepared in-house, and electrosprayed into the instrument with the voltage applied using a platinum wire directly inserted into the solution. Instrument parameters (*SI Appendix*, Table S3) were tuned to minimize gas phase activation and to preserve noncovalent interactions between KRas and SOS^{cat} or SOS^{W729E}. All of the measurements were taken in triplicate and repeated on different days. The mole fractions of free SOS^{cat}, binary and ternary complexes were determined using Unidec software (50) for all triplicates, and average values were used for circle graphs. The additional details on CID, SID, and IM-MS experiments are found in *SI Appendix, Materials and Methods*.

Nucleotide Exchange Assay. The rate of nucleotide dissociation was determined using KRas loaded with BODIPY-GDP in the absence and presence of SOS^{cat} using Clariostar BMG Labtech. The nucleotide exchange was initiated by adding excess amount of GTP ± KRas–GTP, $KRas^{G13D}$–GTP, or $KRas^{Q61H}$–GTP. The details on the assay can be found in *SI Appendix, Materials and Methods*.

Cryo-EM. To obtain the ternary complex of $KRas^{G13D}$ and SOS^{cat}, first $KRas^{G13D}$ was loaded with GppNp (Guanosine 5′-[β,γ-imido] triphosphate trisodium) and excess nucleotide was removed by HiTrap desalting (5 mL; GE) column and concentrated to 15 mg/mL The complex was formed by incubation of threefold molar excess of $KRas^{G13D}$–GppNp with SOS^{cat} for 1 h in ice followed by size-exclusion chromatography to purify the complex to homogeneity. Additional details on data collection for single-particle cryo-EM, image processing, model building, and refinement are available in *SI Appendix, Materials and Methods*.

Data Availability. All study data are included in the article and/or *SI Appendix*.

ACKNOWLEDGMENTS. We thank Dr. John Kuriyan for generously providing plasmids to express SOS fragments. This work was supported by National Cancer Institute (NCI) and National Institute of General Medical Sciences (NIGMS) (Grant R01GM121751), NIGMS (Grant DP2GM123486), and National Institute of Health (NIH) (Grant P41GM128577). Part of this work was performed at the National Center for CryoEM Access and Training and the Simons Electron Microscopy Center located at the New York Structural Biology Center, supported by the NIH Common Fund Transformative High-Resolution Cryo-Electron Microscopy Program (Grant U24 GM129539) and by grants from the Simons Foundation (SF349247) and New York State Assembly.

1. J. Downward, Targeting RAS signalling pathways in cancer therapy. *Nat. Rev. Cancer* **3**, 11–22 (2003).
2. J. Colicelli, Human RAS superfamily proteins and related GTPases. *Sci. STKE* **2004**, RE13 (2004).
3. A. E. Karnoub, R. A. Weinberg, Ras oncogenes: Split personalities. *Nat. Rev. Mol. Cell Biol.* **9**, 517–531 (2008).
4. D. Vigil, J. Cherfils, K. L. Rossman, C. J. Der, Ras superfamily GEFs and GAPs: Validated and tractable targets for cancer therapy? *Nat. Rev. Cancer* **10**, 842–857 (2010).
5. I. A. Prior, P. D. Lewis, C. Mattos, A comprehensive survey of Ras mutations in cancer. *Cancer Res.* **72**, 2457–2467 (2012).
6. A. D. Cox, S. W. Fesik, A. C. Kimmelman, J. Luo, C. J. Der, Drugging the undruggable RAS: Mission possible? *Nat. Rev. Drug Discov.* **13**, 828–851 (2014).
7. A. Fernández-Medarde, E. Santos, Ras in cancer and developmental diseases. *Genes Cancer* **2**, 344–358 (2011).
8. A. G. Stephen, D. Esposito, R. K. Bagni, F. McCormick, Dragging ras back in the ring. *Cancer Cell* **25**, 272–281 (2014).
9. M. V. Milburn *et al.*, Molecular switch for signal transduction: Structural differences between active and inactive forms of protooncogenic ras proteins. *Science* **247**, 939–945 (1990).
10. I. R. Vetter, A. Wittinghofer, The guanine nucleotide-binding switch in three dimensions. *Science* **294**, 1299–1304 (2001).
11. L. Goitre, E. Trapani, L. Trabalzini, S. F. Retta, The Ras superfamily of small GTPases: The unlocked secrets. *Methods Mol. Biol.* **1120**, 1–18 (2014).
12. J. Gureasko *et al.*, Membrane-dependent signal integration by the Ras activator Son of sevenless. *Nat. Struct. Mol. Biol.* **15**, 452–461 (2008).
13. J. M. Rojas, J. L. Oliva, E. Santos, Mammalian son of sevenless Guanine nucleotide exchange factors: Old concepts and new perspectives. *Genes Cancer* **2**, 298–305 (2011).
14. S. M. Margarit *et al.*, Structural evidence for feedback activation by Ras·GTP of the Ras-specific nucleotide exchange factor SOS. *Cell* **112**, 685–695 (2003).
15. H. Sondermann *et al.*, Structural analysis of autoinhibition in the Ras activator Son of sevenless. *Cell* **119**, 393–405 (2004).
16. U. Vo *et al.*, Monitoring Ras interactions with the nucleotide exchange factor son of sevenless (Sos) using site-specific NMR reporter signals and intrinsic fluorescence. *J. Biol. Chem.* **291**, 1703–1718 (2016).
17. M. J. Smith, B. G. Neel, M. Ikura, NMR-based functional profiling of RASopathies and oncogenic RAS mutations. *Proc. Natl. Acad. Sci. U.S.A.* **110**, 4574–4579 (2013).
18. T. S. Freedman *et al.*, Differences in flexibility underlie functional differences in the Ras activators son of sevenless and Ras guanine nucleotide releasing factor 1. *Structure* **17**, 41–53 (2009).
19. L. Iversen *et al.*, Molecular kinetics. Ras activation by SOS: Allosteric regulation by altered fluctuation dynamics. *Science* **345**, 50–54 (2014).
20. J. M. Ostrem, K. M. Shokat, Direct small-molecule inhibitors of KRAS: From structural insights to mechanism-based design. *Nat. Rev. Drug Discov.* **15**, 771–785 (2016).
21. S. Lu, H. Jang, J. Zhang, R. Nussinov, Inhibitors of Ras-SOS interactions. *ChemMedChem* **11**, 814–821 (2016).
22. R. C. Hillig *et al.*, Discovery of potent SOS1 inhibitors that block RAS activation via disruption of the RAS-SOS1 interaction. *Proc. Natl. Acad. Sci. U.S.A.* **116**, 2551–2560 (2019).
23. M. H. Hofmann *et al.*, BI-3406, a potent and selective SOS1-KRAS interaction inhibitor, is effective in KRAS-driven cancers through combined MEK inhibition. *Cancer Discov.* **11**, 142 (2020).
24. G. R. Hilton, J. L. Benesch, Two decades of studying non-covalent biomolecular assemblies by means of electrospray ionization mass spectrometry. *J. R. Soc. Interface* **9**, 801–816 (2012).
25. F. Lanucara, S. W. Holman, C. J. Gray, C. E. Eyers, The power of ion mobility-mass spectrometry for structural characterization and the study of conformational dynamics. *Nat. Chem.* **6**, 281–294 (2014).
26. T. M. Allison, C. Bechara, Structural mass spectrometry comes of age: New insight into protein structure, function and interactions. *Biochem. Soc. Trans.* **47**, 317–327 (2019).
27. A. C. Leney, A. J. R. Heck, Native mass spectrometry: What is in the name? *J. Am. Soc. Mass Spectrom.* **28**, 5–13 (2017).
28. R. S. Quintyn, J. Yan, V. H. Wysocki, Surface-induced dissociation of homotetramers with D2 Symmetry yields their assembly pathways and characterizes the effect of ligand binding. *Chem. Biol.* **22**, 583–592 (2015).
29. J. Gault *et al.*, High-resolution mass spectrometry of small molecules bound to membrane proteins. *Nat. Methods* **13**, 333–336 (2016).
30. R. Daneshfar, E. N. Kitova, J. S. Klassen, Determination of protein-ligand association thermochemistry using variable-temperature nanoelectrospray mass spectrometry. *J. Am. Chem. Soc.* **126**, 4786–4787 (2004).
31. X. Cong *et al.*, Determining membrane protein-lipid binding thermodynamics using native mass spectrometry. *J. Am. Chem. Soc.* **138**, 4346–4349 (2016).
32. J. L. Benesch, F. Sobott, C. V. Robinson, Thermal dissociation of multimeric protein complexes by using nanoelectrospray mass spectrometry. *Anal. Chem.* **75**, 2208–2214 (2003).
33. T. J. El-Baba *et al.*, Melting proteins: Evidence for multiple stable structures upon thermal denaturation of native ubiquitin from ion mobility spectrometry-mass spectrometry measurements. *J. Am. Chem. Soc.* **139**, 6306–6309 (2017).
34. S. A. Raab *et al.*, Evidence for many unique solution structures for chymotrypsin inhibitor 2: A thermodynamic perspective derived from vT-ESI-IMS-MS measurements. *J. Am. Chem. Soc.* **142**, 17372–17383 (2020).
35. X. Cong, Y. Liu, W. Liu, X. Liang, A. Laganowsky, Allosteric modulation of protein-protein interactions by individual lipid binding events. *Nat. Commun.* **8**, 2203 (2017).

36. Z. Moghadamchargari *et al*., Intrinsic GTPase activity of K-RAS monitored by native mass spectrometry. *Biochemistry* **58**, 3396–3405 (2019).
37. S. Lu, H. Jang, R. Nussinov, J. Zhang, The structural basis of oncogenic mutations G12, G13 and Q61 in small GTPase K-Ras4B. *Sci. Rep.* **6**, 21949 (2016).
38. B. E. Hall, S. S. Yang, P. A. Boriack-Sjodin, J. Kuriyan, D. Bar-Sagi, Structure-based mutagenesis reveals distinct functions for Ras switch 1 and switch 2 in Sos-catalyzed guanine nucleotide exchange. *J. Biol. Chem.* **276**, 27629–27637 (2001).
39. J. C. Hunter *et al*., Biochemical and structural analysis of common cancer-associated KRAS mutations. *Mol. Cancer Res.* **13**, 1325–1335 (2015).
40. A. Patgiri, K. K. Yadav, P. S. Arora, D. Bar-Sagi, An orthosteric inhibitor of the Ras-Sos interaction. *Nat. Chem. Biol.* **7**, 585–587 (2011).
41. M. R. Janes *et al*., Targeting KRAS mutant cancers with a covalent G12C-specific inhibitor. *Cell* **172**, 578–589.e17 (2018).
42. F. Shima *et al*., In silico discovery of small-molecule Ras inhibitors that display antitumor activity by blocking the Ras-effector interaction. *Proc. Natl. Acad. Sci. U.S.A.* **110**, 8182–8187 (2013).
43. R. G. Smock, L. M. Gierasch, Sending signals dynamically. *Science* **324**, 198–203 (2009).
44. J. M. Rhett, I. Khan, J. P. O'Bryan, Biology, pathology, and therapeutic targeting of RAS. *Adv. Cancer Res.* **148**, 69–146 (2020).
45. S. Vatansever, B. Erman, Z. H. Gümüş, Comparative effects of oncogenic mutations G12C, G12V, G13D, and Q61H on local conformations and dynamics of K-Ras. *Comput. Struct. Biotechnol. J.* **18**, 1000–1011 (2020).
46. S. Li, A. Balmain, C. M. Counter, A model for RAS mutation patterns in cancers: Finding the sweet spot. *Nat. Rev. Cancer* **18**, 767–777 (2018).
47. H.-H. Jeng, L. J. Taylor, D. Bar-Sagi, Sos-mediated cross-activation of wild-type Ras by oncogenic Ras is essential for tumorigenesis. *Nat. Commun.* **3**, 1168 (2012).
48. J. M. Loree *et al*., Not all RAS mutations created equal: Functional and clinical characterization of 80 different KRAS and NRAS mutations. *J. Clin. Oncol.* **35**, 3589 (2017).
49. W. Y. C. Huang *et al*., A molecular assembly phase transition and kinetic proofreading modulate Ras activation by SOS. *Science* **363**, 1098–1103 (2019).
50. M. T. Marty *et al*., Bayesian deconvolution of mass and ion mobility spectra: From binary interactions to polydisperse ensembles. *Anal. Chem.* **87**, 4370–4376 (2015).
51. C. W. Johnson *et al*., Isoform-specific destabilization of the active site reveals a molecular mechanism of intrinsic activation of KRas G13D. *Cell Rep.* **28**, 1538–1550.e7 (2019).